Prepublished copy

Nature Environment & Pollution Technology

This is a peer-reviewed prepublished version of the paper to be published in Vol. 25, No. 1, March 2026 issue

Type of the Paper (Original Research)

Enhancing S.I. Engine Performance with Metal-Doped Zeolite X Derived from Rice Husk

Aasthiya Bharathinathan[1]†, Karthikeyan Duraisamy[1] and Sethuraman Narayanan[2]

[1]Department of Mechanical Engineering, Annamalai University, Chidambaram, Tamil Nadu, India

[2]Department of Mechanical Engineering, IFET College of Engineering, Villupuram, Tamil Nadu, India

†Corresponding author: Aasthiya B; aasthiyabharathi96@gmail.com

ORCID IDs of Authors: https://orcid.org/0009-0002-4336-1853

Key Words	Synthesis of rice husk, X- zeolite, NOx emission, Catalytic converter
DOI	https://doi.org/10.4649/NEPT.2026.v25i01.B4356 (DOI will be active only after the final publication of the paper)
Citation for the Paper	Bharathinathan, A., Duraisamy, K. and Narayanan, S., 2026. Enhancing S.I. engine performance with metal-doped zeolite X derived from rice husk. *Nature Environment and Pollution Technology*, 25(1), B4356. https://doi.org/10.46488/NEPT.2026.v25i01.B4356

ABSTRACT

The increasing prevalence of harmful NOx emissions from gasoline engines necessitates the development of alternatives to traditional three-way catalytic converters. This study investigates the potential of low-cost zeolites derived from rice husk ash as a promising alternative. Na-X zeolites derived from rice husk ash were characterized using X-ray fluorescence (XRF), Fourier-transform infrared spectroscopy (FTIR), X-ray diffraction (XRD), and field emission scanning electron microscopy (FESEM) to determine their structural properties and morphology. These zeolites were then modified with copper (Cu) and iron (Fe) ions to create Cu-X and Fe-X zeolite catalysts. The catalysts were wash-coated onto cordierite honeycomb monoliths and integrated and properly housed in a steel casing catalytic converter and fitted near to the exhaust manifold of twin-cylinder nano-engine. Engine performance and emissions were evaluated under various operating loads (4, 7, 10, 13, and 16 kW). NOx, CO, HC, CO_2, and O_2 emissions were measured using an AVL DI gas analyzer. The results demonstrated that the developed Cu-X and Fe-X zeolite converters significantly outperformed the conventional catalytic converter in reducing NOx emissions, while maintaining comparable performance for other pollutants. The enhanced NOx reduction capabilities of the zeolite catalysts can be attributed to their unique structural properties and the synergistic effect of the copper and iron ions.

INTRODUCTION

Zeolites, synthetic crystalline aluminosilicates, have become indispensable across various industries due to their unique structural properties and remarkable performance. Zeolite X, in particular, features a three-

dimensional framework of interconnected tetrahedral units composed primarily of silicon (Si) and aluminum (Al) atoms. These tetrahedra are linked by oxygen atoms (O), forming a network of channels and cavities that define the material's high surface area and ion-exchange capabilities.

The discovery of zeolites dates back to 1756 when Cronstedt identified stilbite—the first known zeolite—after observing its rapid water loss upon heating, resembling boiling. The term "zeolite" originates from the Greek words zeo (to boil) and lithos (stone) (Edanol, Y. et al., 2018). Zeolites typically follow the empirical formula $M_2/Al_2O_3 \cdot xSiO_2 \cdot yH_2O$, where M represents an exchangeable cation with valence n. Commonly, M includes Group I or II ions, though other metal, non-metal, and organic cations may also be used to balance the negative charge introduced by aluminum in the structure (Saceda J. J. et al., 2011).

Rice husk, an abundant agricultural byproduct, consists mainly of the husk along with rice straw, plant matter, and other organic components. Significantly, rice husk contains over 90% silica, making it a cost-effective and plentiful source of high-quality amorphous silica. Extensive research has been devoted to extracting silica from rice husk for various applications, including the production of nano-silica (Ma et al., 2014). Silica's versatility enables its use in a wide range of industries, such as ceramics, chromatography, adhesives, detergents, electronics, pharmaceuticals, and vegetable oil processing. Rice husk ash (RHA), produced by burning rice husk, has gained attention as a low-cost raw material for synthesizing silica powders and gels (Das et al., 2022). However, silica extracted from RHA may contain impurities like CaO, Al_2O_3, and MgO in addition to SiO_2. These impurities must be considered and, if necessary, removed depending on the intended application (Hassan et al., 2021).

Several studies have focused on synthesizing zeolites from RHA-derived silica. Dalai et al. (2010) synthesized zeolites such as NaX, PC, analcime, and hydroxysodalite using standard procedures and reported evidence of new phase formation at elevated temperatures through XRD analysis. Yusof et al. (2011) successfully synthesized high-purity Zeolite NaY at a controlled temperature of 600°C, utilizing seeding and aging processes to eliminate undesired phases. Saceda et al. (2012) compared silica extraction from both rice husk (RH) and RHA, concluding that RH is a more efficient source for Zeolite NaY synthesis due to simpler extraction and higher recovery. Silica from RH consisted solely of SiO_2, while that from RHA contained 97.56% SiO_2 along with 2.14% K_2O and 0.31% Al_2O_3. The resulting Zeolite NaY exhibited a high BET surface area of 882 m^2/g and a micropore volume of 0.38 cm^3/g, typical of Y-type zeolite structures. Setthaya

et al. (2013) synthesized faujasite and analcime zeolites using RHA and metakaolin through a dissolution-precipitation method followed by hydrothermal treatment. They found that faujasite formed at lower hydrothermal temperatures, whereas analcime developed under higher temperatures and prolonged synthesis durations. They concluded that time and temperature affect phase transitions and crystal development, while stirring duration impacts specific surface area but not zeolite type. Santasnachok et al. (2014) synthesized pure Na-A and Na-X zeolites using alkali fusion followed by extraction, residue removal, and hydrothermal treatment. Zeolite A was synthesized at 90°C for 10 to 24 hours using Si/Al molar ratios of 0.5 to 1.0. NaX zeolite was produced under the same conditions with Si/Al ratios ranging from 1.5 to 2.0. Both zeolites were tested for cadmium ion removal, with Na-A proving more effective, reducing Cd^{2+} concentrations below the WHO limit of 0.01 mg/L. Pandiangan et al. (2015) reported successful synthesis of zeolite X from rice husk silica and aluminum, confirmed by Fourier-transform infrared (FTIR), X-ray diffraction (XRD)**,** and Field emission Scanning Electron Microscopy (FESEM) analysis. Furthermore, transesterification experiments verified by GC-MS demonstrated the catalytic activity of zeolite X in converting palm oil into biodiesel.

Substantial research has explored the influence of varying hydrothermal conditions on zeolite synthesis (Saleh et al., 2018). The literature consistently supports alkali fusion combined with hydrothermal treatment as an efficient strategy for producing various zeolite types—such as X, Y, NaX, NaY, NaP, PC, analcime, and hydroxysodalite—from rice husk ash with different compositions.The central problem addressed in this study is the substantial emission of nitrogen oxides (NOx) from gasoline engines, which significantly contributes to air pollution and poses serious environmental and health risks. Traditional catalytic converters often show limited effectiveness under the oxygen-rich conditions typical of gasoline engine exhaust. Hence, there is a pressing need for more efficient and sustainable catalysts. The primary objective of this research is to develop novel zeolite-based catalysts synthesized from rice husk ash, an eco-friendly and low-cost silica source. These zeolites are further modified with copper and iron ions to improve their catalytic performance for NOx reduction. The study aims to assess the effectiveness of Cu-X and Fe-X catalysts under different engine operating conditions and compare their performance with conventional catalytic converters. Ultimately, this research aspires to contribute to cleaner emission control technologies for gasoline engines, supporting the advancement of more environmentally friendly transportation systems.

2. MATERIALS AND METHODS

The best raw material of rice husk (RH) used for the production of zeolites-x. By initially, the formation of zeolites-X from silica, therefore silica produced by the acid treatment of RH during incineration. Here the main precursor for the synthesis of the silica source is dissolved rice husk. Raw rice husks undergo a multi-step purification process to yield a refined ash product. Initially, the husks are sieved to remove impurities like clay and dust. Following this, they are steeped in a 10M concentrated hydrochloric acid solution. The treated husks are then thoroughly washed, filtered, and air-dried. The final step involves calcination at 850°C for five hours. Initially 50g of silica and 20 of sodium hydroxide were dissolved into 500 ml of distilled water. Then the mixture was agitator with a magnetic stirrer. After a little while, the required amount of 10g of sodium hydroxide and 10g of aluminum oxide were both dissolved in separate beaker, in addition to the solution form into sodium aluminate the pH value is 11 occur seems to bluish color. The mixture of sodium aluminate dissolved in silicate solution. Stir well until 4hrs around 250 rpm the silica dissolves clearly. At last the sample is obtained. Take it out and wash it several times until the impurities remove. The obtained place in the oven at 100°C for 24 hr. At last the obtained zeolite x like material.

2.1 XRF

The elemental composition of the raw rice husk (RRH) and the synthesized zeolite X was determined using X-ray fluorescence (XRF) spectroscopy. The Table 1 revealed a significant increase in the silica (SiO_2) content from 59.57 wt.% in RRH to 67.612 wt.% in the final zeolite X product, indicating the successful enrichment of silica during the synthesis process. Silica (SiO_2) forms the primary framework of zeolite X, consisting of tetrahedral coordinated silicon atoms linked by oxygen atoms to create a three-dimensional network. Alongside SiO_2, sodium oxide (Na_2O) and aluminium oxide (Al_2O_3) constitute the fundamental components of the zeolitic structure. Notably, Na_2O was present at 8.789 wt.% in the synthesized material, balancing the negative charge introduced by Al atoms within the framework. These sodium ions are located within the pores of the zeolite and are exchangeable with other cations such as K^+, Ca^{2+}, and Mg^{2+}, providing versatility for ion exchange and catalytic applications. The presence of Al_2O_3 further enhances the structural stability and acidic properties of the material, which are crucial for catalytic performance. Additionally, trace quantities of K_2O, CaO, TiO_2, and Fe_2O_3 were detected in the final product. These minor oxides may contribute to the modulation of the zeolite's physicochemical and catalytic behavior.

METAL OXIDES	RRH %	IN HOUSE MADE ZE-OLITE X%
SiO_2	59.57	67.612
Al_2O_3	3.58	15.675
Na_2O	0.58	8.789
P_2O_5	18.85	1.789
K_2O	6.85	0.9
CaO	1.95	0.971
TiO_2	0.24	0.303
Fe_2O_3	0.14	4.476
MgO	4.58	0.00
Cl	0.58	0.00
SO_3	3.08	0.00
MoO_3	0.02	0.00

Table: 1 the Elemental Composition of Zeolite X

2.2 FTIR

FTIR spectroscopy was employed to analyze the functional groups and structural features of the synthesized zeolite X. The Fig.1 revealed characteristic absorption bands that are consistent with the framework vibrations of zeolitic materials. A strong and broad peak near 1000 cm^{-1} corresponds to the asymmetric stretching vibrations of Si–O–Si**,** confirming the formation of the zeolite's tetrahedral silica framework. A distinct signal observed at 880 cm^{-1} is attributed to internal ring vibrations**,** which are typically associated with specific pore structures and crystalline arrangements within zeolite frameworks. A broad band around 3000 cm^{-1} indicates the presence of hydroxyl (–OH) groups**,** likely arising from adsorbed silanol species or water molecules on the surface. The presence of water is further supported by a peak near 1800 cm^{-1}**,** which is attributed to bending vibrations of molecularly adsorbed H_2O**.** An additional feature at approximately 2350 cm^{-1} is ascribed to adsorbed atmospheric CO_2**,** commonly seen in FTIR spectra of porous materials exposed to ambient air. Moreover, C–H stretching bands overlapping around 3000 cm^{-1} suggest the presence of residual organic species from synthesis or precursor materials. The high transmittance observed in the 4000–5000 cm^{-1} region

indicates the absence of significant absorption bands in this range, confirming the structural purity of the sample. Overall, the FTIR data validate the successful synthesis of zeolite X and reflect its compositional and structural fidelity.

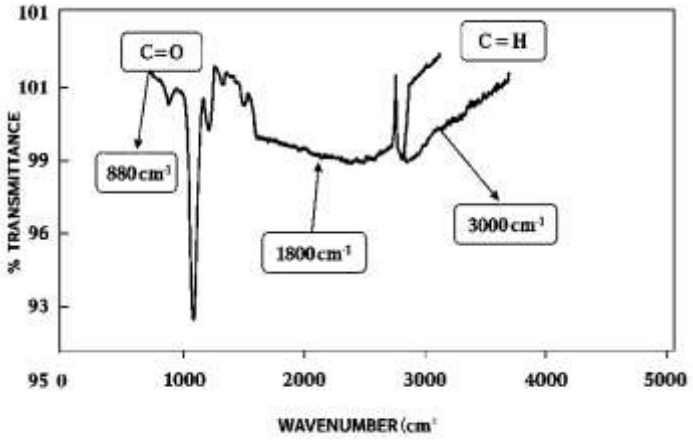

Fig: 1 FTIR Diffraction of in House Made Zeolite X

2.3 FESEM

FESEM was employed to investigate the surface morphology and microstructure of the synthesized zeolite X. As shown in Fig .2 the sample consists of relatively small particles with an average size in the ~1 μm range**,** which aligns well with typical zeolite particle size distributions. The particles exhibit an irregular and porous morphology**,** featuring a honeycomb-like framework with interconnected pores**,** characteristic of zeolite X. This microstructure is beneficial for catalytic applications due to enhanced surface area and accessibility to active sites. Slight aggregation of particles was observed, Fig.3 shows potentially caused by electrostatic interconnect during the synthesis and drying processes. Moreover, the particle surfaces appear rough and textured, suggesting the presence of surface defects or structural irregularities**,** which can significantly influence the material's adsorption and catalytic performance**.** These morphological features collectively confirm the successful formation of zeolite X with a structure suitable for advanced catalytic applications.

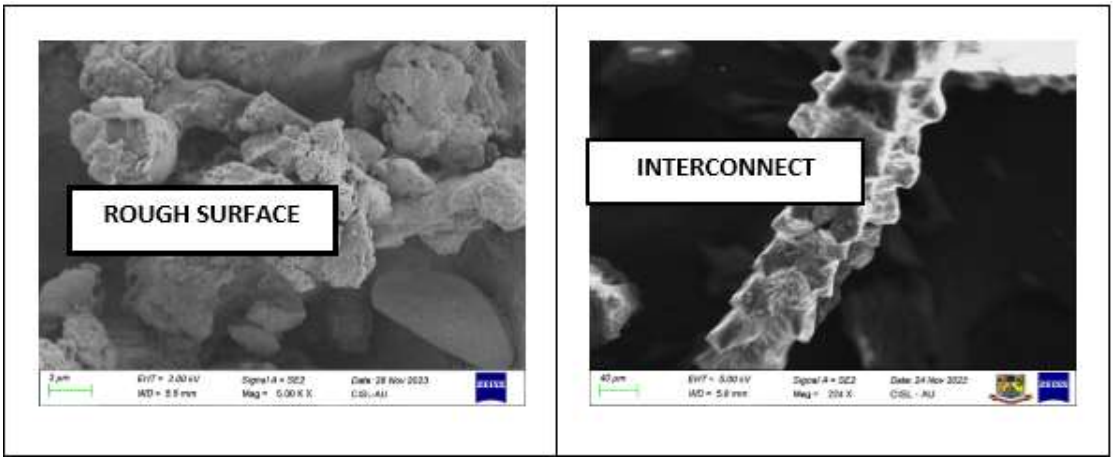

Fig: 2 and 3 Morphology of Raw rice husk and the morphology of in house- made zeolite x

2.4 Preparation of Cu-X and Fe-X Zeolite Catalysts

Cu-X and Fe-X zeolite catalysts were synthesized via ion-exchange of zeolite X, followed by Washcoating onto cordierite monoliths using a silica-based slurry to achieve 15 wt.% coating and thermal activation.

To prepare the metal-exchanged zeolite catalysts, 10 g of zeolite X powder synthesized from rice husk ash was subjected to an ion-exchange process. The powder was dispersed in 1000 mL of 0.05 M cupric chloride dihydrate ($CuCl_2 \cdot 2H_2O$, Fisher Scientific) solution and stirred vigorously using a magnetic stirrer at ambient temperature for 24 h. The suspension was vacuum-filtered and rinsed thoroughly with deionized water to remove excess ions. For the Fe-exchanged zeolite, ferrous chloride tetrahydrate ($FeCl_2 \cdot 4H_2O$, Fisher Scientific) was used instead of cupric chloride. The resulting solids were dried in an oven and calcined at 550 °C for 6 h to activate the catalysts.

Cordierite monoliths (supplied by Bocent Advanced Ceramics Co., Ltd.) were used as substrates. These monoliths had a cell density of 400 CPSI, a wall thickness of 0.17 mm, and were 90 mm in both diameter and length. One monolith was platinum-coated, and the other was uncoated, serving as a control.

The washcoating slurry consisted of 20 wt. % Cu-X zeolite, 4 wt. % silica gel, and distilled water as the solvent. Each monolith was dipped in the slurry for one minute and excess slurry was blown out with compressed air through both ends. The monoliths were dried in a muffle furnace at 120 °C for 2 h, and the process was repeated until the washcoat loading reached 15 wt.% of the monolith's weight. Finally, the coated monoliths were calcined at 500 °C for 5 h. The same Washcoating and thermal treatment protocol was applied to prepare Pt-Fe-zeolite and Fe-X zeolite-coated monoliths.

2.5 Fabrication of Catalytic Converter – Catalytic activity tests on a twin-cylinder petrol engine were conducted using two fabricated catalytic converter types.

Type1:

Two catalytic converters were fabricated with dimensions matching the original equipment manufacturer's catalytic converter. A Pt-Cu-X zeolite-coated monolith was tightly wrapped with resilient matting (to dampen vibrations) and then mounted in a steel casing. Inlet and outlet cones were welded to both ends of the casing. The catalytic converter was firmly attached to the engines exhaust pipe. A stainless steel cover acted as a heat shield. Pt-Fe- coated monolith catalytic converters were fabricated using the same procedure. Fig: 4 shows the in house and commercial catalytic converters respectively.

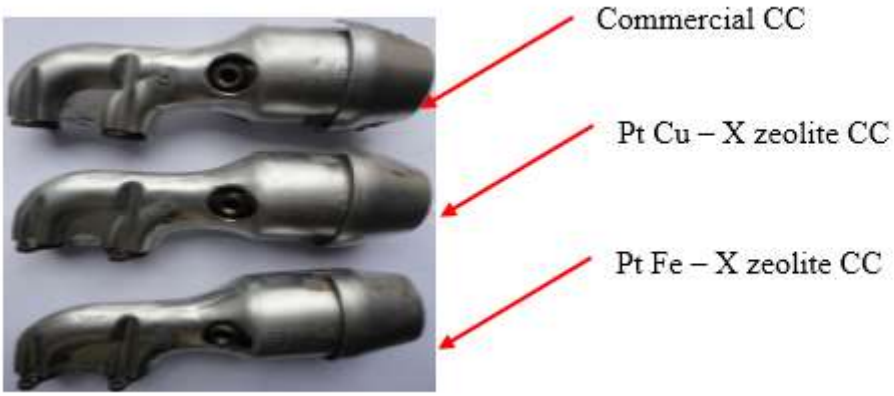

Fig: 4 Photographic view in-house made and commercial catalytic converter

Type 2:

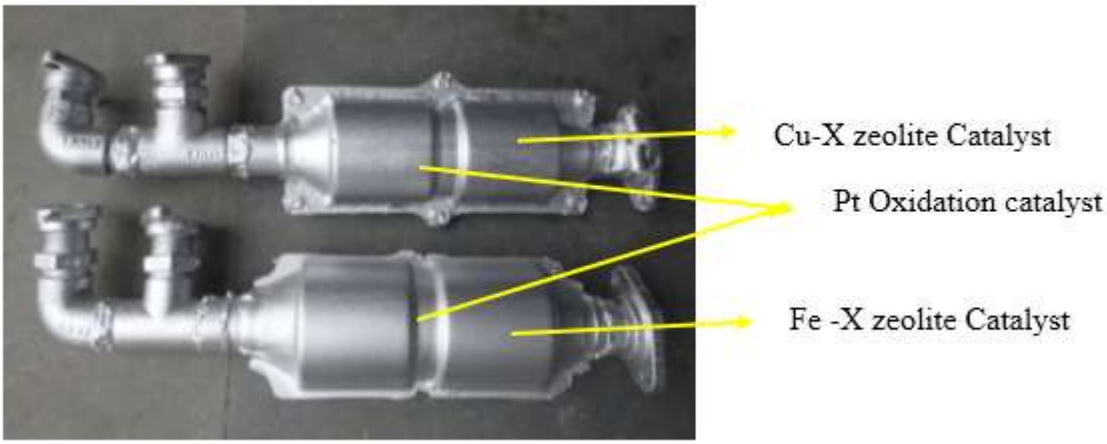

Fig: 5 Depiction of the In-House Built deNOx Catalytic Converter

For the different configuration, a commercially sourced platinum (Pt)- coated monolith and a conventionally prepared copper- exchanged zeolite x (Cu-X) coated monolith were meticulously assembled within a welded steel casing, accomplish with integrated inlet and outlet cones. This design strategically combined the catalytic activity of the Pt- coated monolith with the NOx reduction capabilities of the (Cu-X) zeolite coating. To ensure secure installation within the engine's exhaust system, appropriate mounting provisions were incorporated. A similar fabrication process was employed to create a catalytic converter utilizing a Pt-coated monolith and an iron-exchanged zeolite X (Fe-X) coated monolith. The above Fig.5 depicts the deNOx catalytic converter, which was manufactured in-house. The second configuration involved the assembly of a commercially obtained platinum-coated monolith and a custom-prepared copper-exchanged zeolite X (Cu- X) coated monolith within a steel casing. This casing was then proficiently welded and fitted with inlet and outlet cones to facilitate gas flow. The resulting catalytic converter was securely integrated into the engine's exhaust pipe. A parallel fabrication process was used to create a separate catalytic converter, this time combining a platinum-coated monolith with an iron-exchanged zeolite X (Fe-X) coated monolith. it shows a visual representation of the deNOx catalytic converter, which was produced within our own facilities.

2.6. EXPERIMENTAL SETUP

Type	Vertical In-line Engine with MPFI
Number of cylinders	2
Displacement	624 cc
Bore	73.5 mm
Stroke	73.5 mm
Compression Ratio	9.5:1
Fuel	Petrol
Cycle	4-Stroke
Max. Engine output	25.74 kW @ 5250 rpm
Max. Torque	48 Nm @ 3000 rpm
Speed	2500 rpm
Orifice Diameter	20 mm
Cooling System	Water
Loading Device	Eddy current dynamometer

TABLE: 2 SPECIFICATION OF PETROL ENGINE

The test engine for this research was a 624 cc, four-stroke, twin-cylinder, water-cooled spark-ignition type. Fig.6 and the accompanying table describe the test facility, which comprised the engine fixed on a test bed and directly linked to an eddy current dynamometer. This dynamometer provided precise engine loading control and switching capabilities. The experiment used an AVL-Di gas analyzer utilized for the accurate measurement of CO, HC, NOx, and O_2 emissions. Exhaust gas temperatures were monitored using strategically placed Chromel-Alumel thermocouples at three distinct locations on the converter.

Initially, standard engine performance was established by operating the engine without a catalytic converter across a range of loads (4, 7, 10, 13, and 16 kW) while sustaining a constant speed of 2500 rpm. Emissions of HC, CO, CO_2, O_2, and NOx were methodically recorded for each load condition. Thereafter, Fig.7 a commercially available catalytic converter was Affixed on the engine exhaust manifold, ensuring axial entry of the exhaust gases. The engine was then operated under the Equivalent load and speed conditions previously used for the baseline measurements, and emissions of HC, CO, CO_2, O_2 and NOx were again recorded. This comparative testing procedure was replicated using both the Fe-zeolite and Cu-zeolite converters. Emissions measurements were conducted under the same operating conditions to rigorously evaluate the performance of these in-house fabricated converters against the commercially available unit.

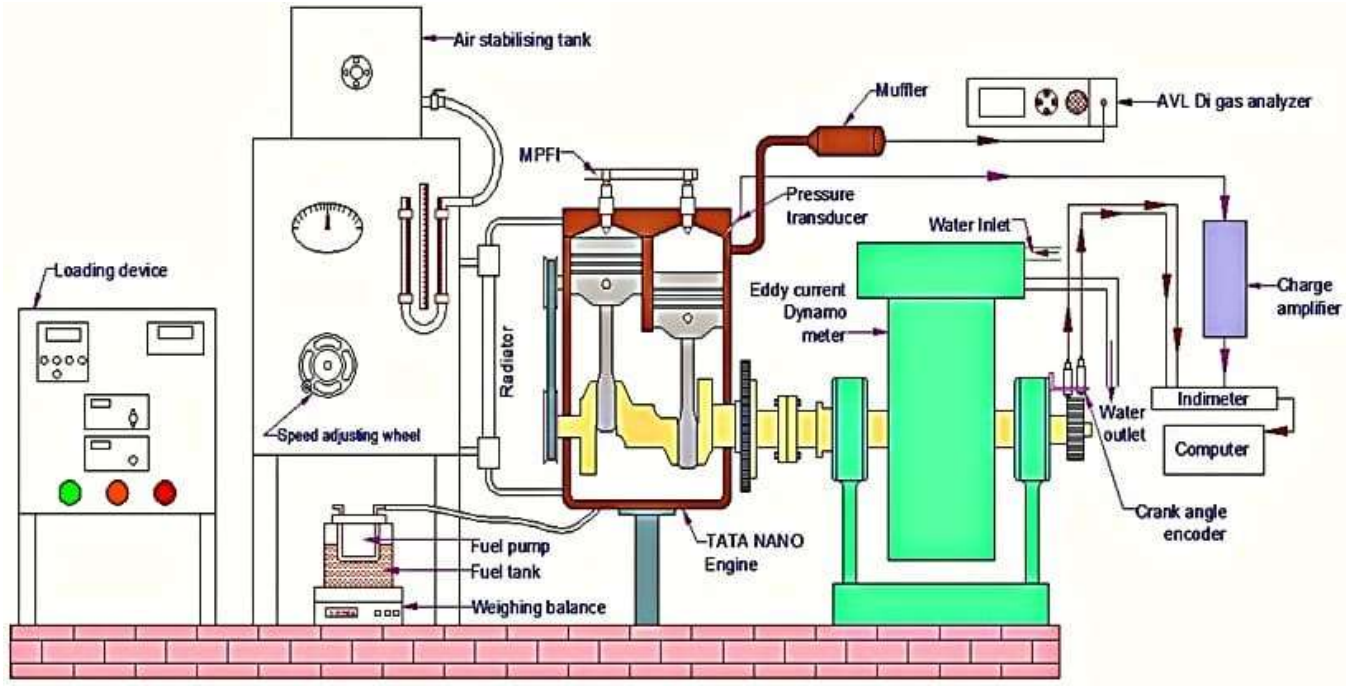

Fig: 6 Experimental setup of petrol engine

Fig: 7 Photographic view of catalytic converter fitted in engine

3. RESULT AND DISCUSSION

A twin-cylinder, MPFI petrol engine, connected to an eddy current dynamometer, was used for the experiments. The conversion efficiencies were then determined using the following calculations:

- NOx Conversion Efficiency = (Inlet NOx - Outlet NOx) / Inlet NOx * 100
- HC Conversion Efficiency = (Inlet HC - Outlet HC) / Inlet HC * 100
- CO Conversion Efficiency = (Inlet CO - Outlet CO) / Inlet CO * 100

3.1 Nitrogen oxides emission with load

The Figs.8 and 9 demonstrate the NOx reconfiguration efficiency at various engine loads. The data clearly demonstrate that all in-house developed catalytic converters achieve significantly higher NOx change than the commercial converter. This effectiveness arises because commercial catalytic converters are designed for stoichiometric air-fuel ratios. However, the engine used lean-burn Multi Point Fuel Injection (MPFI) engine, resulting in oxygen-rich exhaust, which negatively enhance the efficiency of conventional converters. To resolve, a more effective catalytic system utilizing zeolite x was developed to diminish NOx emissions. Zeolite active sites exhibit a high affinity for NO, facilitating its separation into nitrogen (N) and oxygen (O). As shown in this results in enhanced conversion efficiency with the introduce system. In this figs. 8 and 9 seems that the double-layer monolith catalytic converters (Pt-Cu-X zeolite and Pt-Fe-X zeolite) which emphasizes the lower quality of the outcomes than the combined monolith catalytic converters (Pt & Cu- X Zeolite and

Pt & Fe-X zeolite). Notably, the Pt-Fe-X zeolite converter achieves approximately 50% NOx conversion at a 4 kW load, gradually increasing to about 59% at 16 kW. In contrast, the Pt & Fe-X zeolite converter reduces NOx by roughly 55% at 4 kW and 70% at 16 kW.

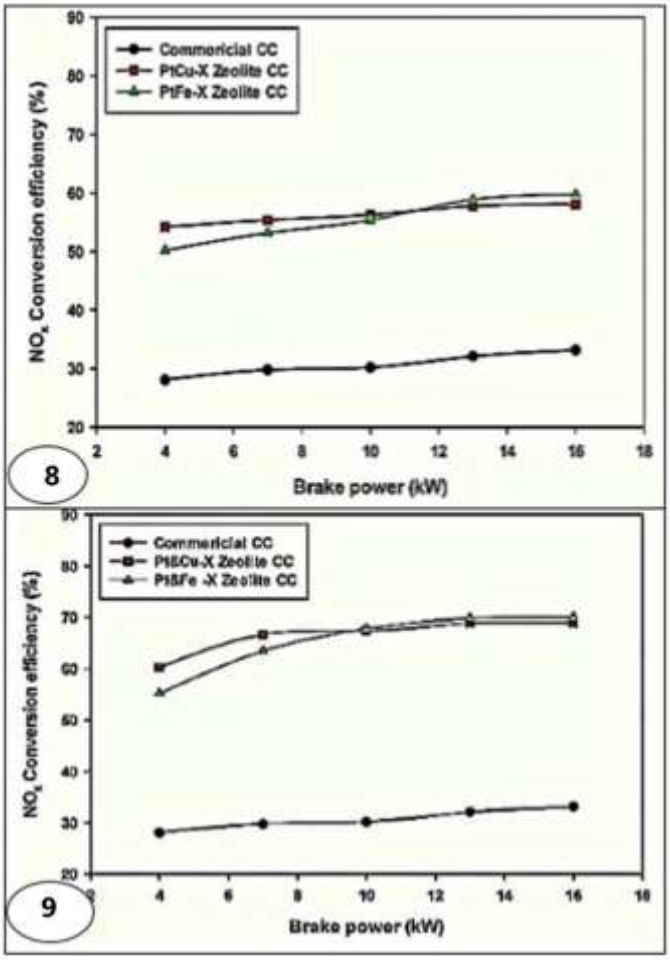

Fig: 8 &9 Percentage reduction of NOx Vs. load (dual layer) and Percentage reduction of NOx Vs. load (deNO*x*)

Here's a paraphrase of the provided text, aiming for clarity and conciseness: The dual-layer catalytic converter's performance is limited because it requires simultaneous reactions of CO, HC, and NOx, restricting NOx reduction to the channel corners. Distinctly, the combined Pt and Fe –x zeolite monolith catalyst offer more active sites, enhancing NOx conversion. This occurs as exhaust gas flows through the platinum monolith, facilitating NO decomposition into adsorbed nitrogen and oxygen. The nitrogen atoms then combine to form N2 and the oxygen reacts with CO to produce CO2. However, at a 4 KW load, the Pt and Cu-X zeolite catalyst showed superior performance compared to the Pt-Fe-X zeolite catalyst

This performance difference can be attributed to the fact that three reactions (the reduction of CO, HC, and NOx to CO_2, H_2O, and N_2) occur simultaneously within the dual-layer catalytic converter, limiting the active NOx reduction sites to the corners of the monolith channels. The combined monolith catalytic converter (Pt & Fe-X) provides more active sites for NOx conversion, leading to improved performance. As exhaust gas passes through the platinum (Pt) monolith and subsequently contacts the deNOx monolith, the following reactions occur: (i) NO is adsorbed onto the active metal sites and dissociates into adsorbed nitrogen (N (ads)) and oxygen (O (ads)), (ii) two N (ads) atoms combine to form N_2, and (iii) the dissociated O (ads) reacts with the remaining CO in the exhaust gas to produce CO_2. At a 4 kW load, the Pt & Cu-X catalytic converter demonstrated better performance than the Pt & Fe-X catalytic converter.

3.2 Effects of Exhaust Gas Temperature on Nitrogen Oxide Emission Levels

The relationship between exhaust gas temperature and NOx conversion efficiency is compared in Fig.10 and 11. The dual-layer catalytic converter demonstrates a progressive, albeit gradual, increase in efficiency, achieving a 50% NOx conversion rate at approximately 300°C. Conversely, the combined monolith catalytic converter (deNOx) exhibits a remarkably rapid surge in conversion efficiency, attaining a 60% conversion rate at approximately 190°C. This enhanced performance continues to improve steadily up to 500°C, beyond which any further significant enhancements are negligible. It is well-established that catalytic converter efficiency is profoundly influenced by temperature. It is expected that the zeolite catalyst will begin to function at approximately 180°C. Below 150°C, its catalytic activity decreases. However, exceeding 180°C triggers a notable activation of the zeolite, resulting in a substantial improvement in NOx conversion efficiency. This temperature-dependent behavior is conspicuously absent in conventional commercial converters, which often struggle to achieve effective NOx reduction in oxygen-rich exhaust environments.

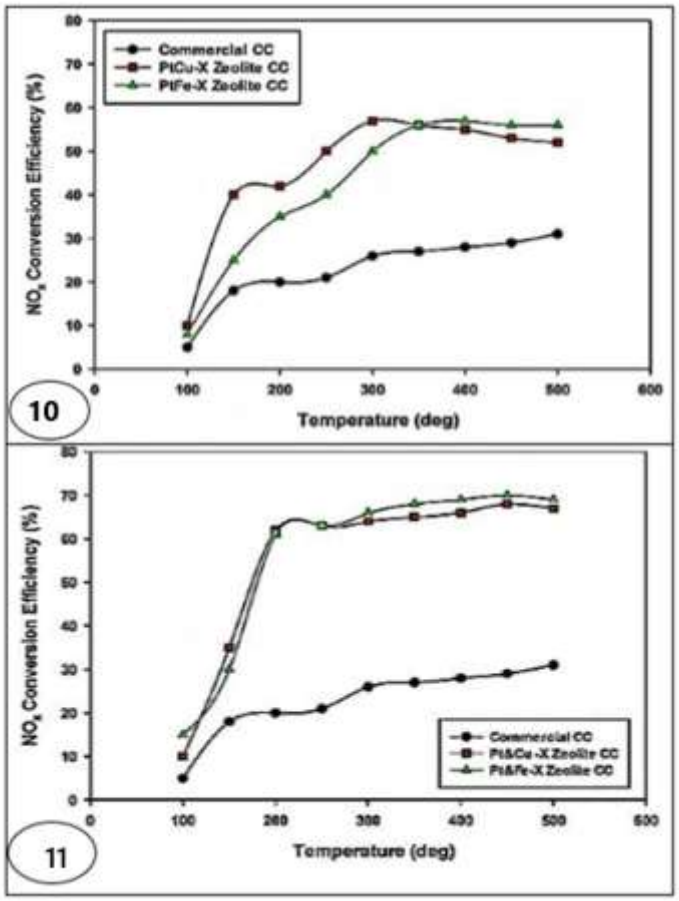

Fig: 10 &11 Percentage reduction of NOxVs. Temperature (dual layer) and Percentage reduction of NOxVs. Temperature (deNO*x*)

3.3 Co Conversion Efficiency

Fig: 12 and 13 seems the CO conversion efficiencies of both the dual-layer monolith catalytic converter and the deNOx catalytic converter. Previous studies (Alkaemade et al, 2006 and Santos et al, 2008) have shown that commercial monoliths effectively reduce CO and HC emissions under lean exhaust conditions. Fig.12 denotes only a slight decrease in CO changeover efficiency compared to the commercial catalytic converter. This is likely because the platinum (Pt) layer in the dual-layer monolith is partially obscured by the zeolite layer, reducing the number of active sites available for CO conversion.

Fig.13 illustrate that the deNOx catalyst achieves approximately 93% CO conversion efficiency at a 4 kW load, enhancing to nearly 95% at 16 kW. The improved performance is due to residual CO from the Pt-coated monolith reacting with adsorbed oxygen on the deNOx catalyst, resulting in CO_2 formation. Prior studies have shown that CO oxidation aids NOx reduction in metal exchanged zeolite catalysts.

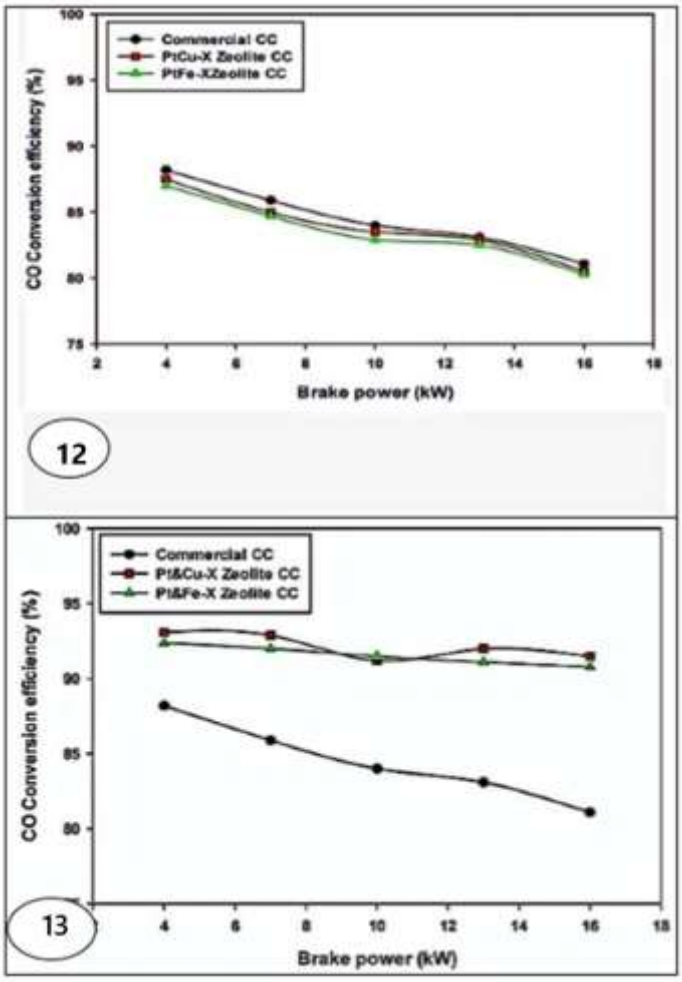

Fig: 12 &13 Carbon monoxide against brake power (dual layer) and Carbon monoxide against brake power (deNO*x*)

3.4 Efficiency of Hydrocarbon conversion

Figs .14 and 15 show the percentages reduction in HC emissions as a function of engine brake power. The dual –layer catalytic converter achieves 72% HC conversion at a 4kW load, increasing to 79% at 16Kw. The deNOx converter system, however, achieves approximately 90% HC conversion at 4 kW, rising to 93% at 16 kW. This higher conversion is attributed to the reaction of unreacted HC emissions exiting the Pt-coated catalyst with adsorbed oxygen, producing CO_2 and H_2O. As demonstrated in earlier work (Kaspar et al., 2003; Liu et al., 2004), hydrocarbons act as reducing agents by removing adsorbed oxygen generated during NOx dissociation. This action preserves the reduced states of the active sites (Cu^+ or Fe^+), which facilitates further NOx reduction.

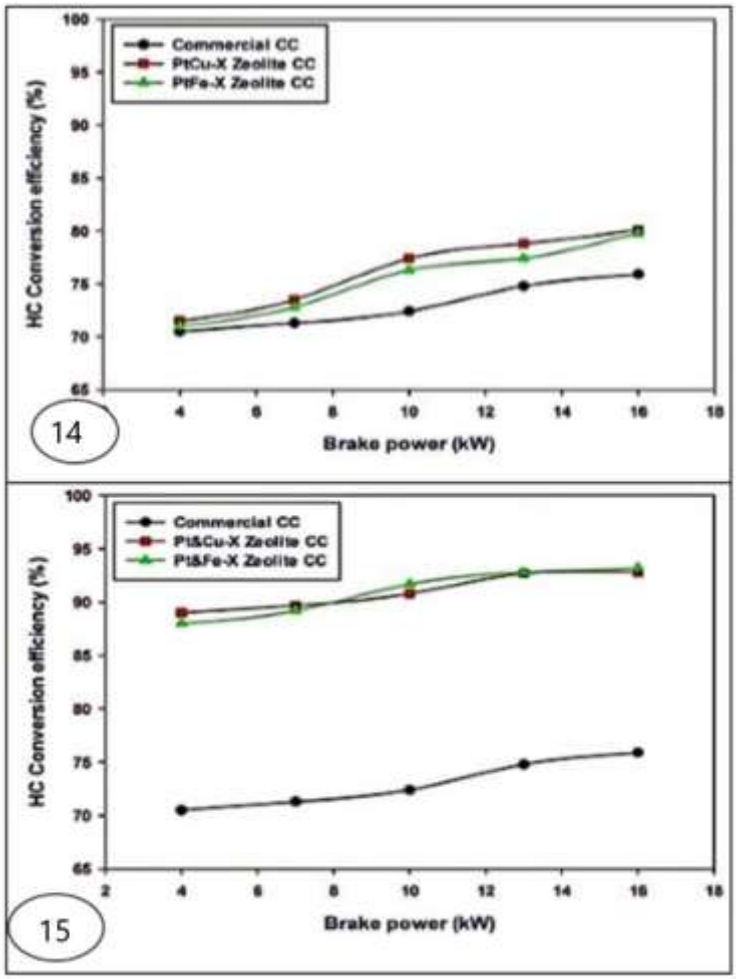

Fig: 14 &15 Hydrocarbon against brake power (dual layer) and Hydrocarbon against brake power (deNO*x*)

3.5 Brake thermal efficiency

Fig.16 and 17 present a comparative analysis of the engine's thermal efficiency in relation to its brake power output. A subtle yet discernible reduction in brake thermal efficiency is observed when employing the dual-layer monolith catalytic converter, as opposed to the commercially available counterpart. This diminution can be attributed to the marginally increased flow resistance encountered by the exhaust gases as they traverse the monolith walls. The introduction of an additional wash coating layer within the monolith channels effectively reduces the overall flow area, thereby impeding gas flow. Conversely, the deNOx system demonstrates a brake thermal efficiency that closely mirrors that of the commercial catalytic converter. Notably, despite the inclusion of two distinct monoliths, the deNOx system does not introduce any significant flow resistance within the exhaust gas pathway.

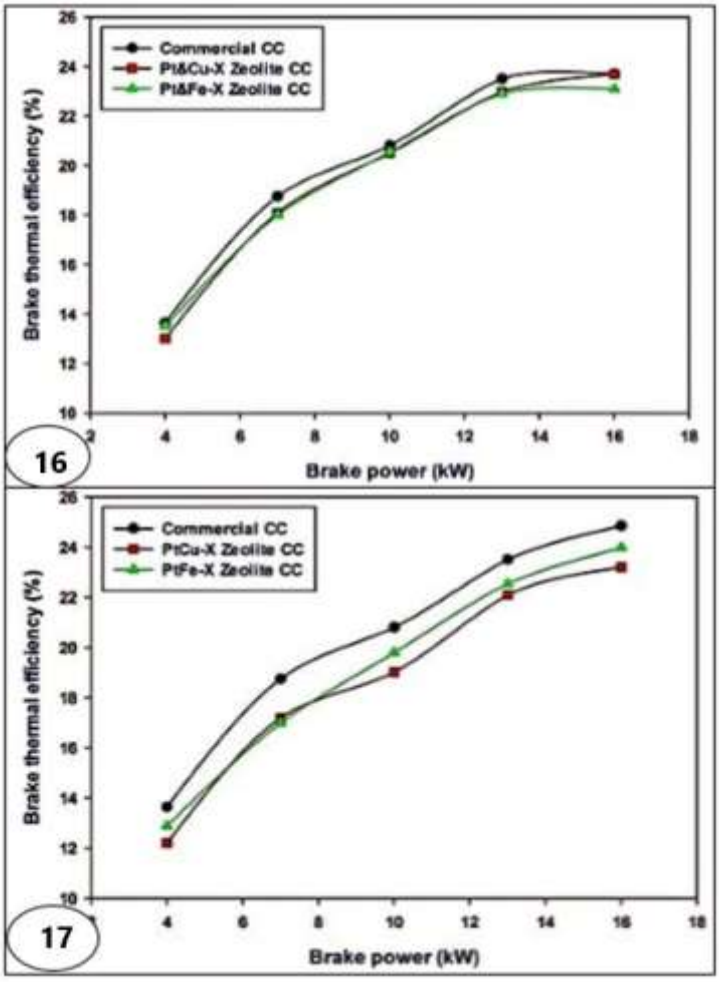

Fig: 16 &17 Brake thermal efficiency against brake power (dual layer) and deNOx Performance: Brake Thermal Efficiency as a Function of Brake Power

4 . CONCLUSION

This study suggests a potential alternative to conventional three-way catalytic converters for reducing NOx emissions from gasoline engines. The synthesized rice husk ash-based Na-X zeolite catalysts, modified with copper and iron ions (Cu-X and Fe-X), demonstrated superior NOx reduction compared to the conventional converter while maintaining comparable performance for other pollutants. The enhanced performance can be attributed to the unique structural properties of the zeolite-based catalysts and the synergistic effect of the copper and iron ions. These findings indicate that the developed Cu-X and Fe-X zeolite catalysts show promise as a cost-effective and environmentally friendly option for reducing NOx emissions from gasoline engines. Further research and development are needed to optimize their

- ✓ The custom-made metal-doped X zeolite converter outperformed the commercially available one. Performance and scale up production for commercial applications.
- ✓ Copper-X zeolite was more effective at reducing NOx in cooler conditions, whereas iron-X zeolite excelled at higher temperatures.

- ✓ Both carbon monoxide and hydrocarbon emissions were substantially lowered across all engine loads and during speed variation tests.
- ✓ The catalyst bed did not create excessive back pressure.
- ✓ The catalytic converter showed no noticeable loss of activity after 50 hours of testing.

Conflicts of interest

The authors declare no conflicts of interest.

Acknowledgement

The researchers expressed their gratitude to Annamalai University, department of Mechanical Engineering, Research lab. so that it can run well and get results that can benefit the academic world.

REFERENCES

1. Al-Jubouri, S. M., Al-Batty, S. I., & Holmes, S. M. (2021). Using the ash of common water reeds as a silica source for producing high purity ZSM-5 zeolite microspheres. *Microporous and mesoporous materials*, *316*, 110953. https://doi.org/10.1016/j.micromeso.2021.110953.
2. Chen, C., Cai, L., Zhang, L., Fu, W., Hong, Y., Gao, X., & Wu, G. (2020). Transesterification of rice bran oil to biodiesel using mesoporous NaBeta zeolite-supported molybdenum catalyst: Experimental and kinetic studies. *Chemical Engineering Journal*, *382*, 122839. https://doi.org/10.1016/j.cej.2019.122839.
3. Chen, J., & Lu, X. (2018). Synthesis and characterization of zeolites NaA and NaX from coal gangue. *Journal of Material Cycles and Waste Management*, *20*, 489-495. https://doi.org/10.1007/s10163-017-0605-5.
4. Dalai, A. K., Rao, M. S., & Gokhale, K. V. G. K. (1985). Synthesis of NaX zeolite using silica from rice husk ash. *Industrial & engineering chemistry product research and development*, *24*(3), 465-468. https://doi.org/10.1021/i300019a026.
5. Das, S. K., Adediran, A., Kaze, C. R., Mustakim, S. M., & Leklou, N. (2022). Production, characteristics, and utilization of rice husk ash in alkali activated materials: An overview of fresh and hardened state properties. *Construction and Building Materials*, *345*, 128341. https://doi.org/10.1016/j.conbuildmat.2022.128341.
6. Edanol, Y., Usman, K., Buenviaje, S., Mantua, M., & Payawan, L. (2018). Utilizing silica from rice hull for the hydrothermal synthesis of zeolite Y. *KIMIKA*, *29*(1), 17-21. DOI:10.26534/kimika.v29i1.17-21.
7. Farirai, F. (2020). *Production of Nano silicon particles from sugarcane bagasse ash for solar cell application* (Doctoral dissertation, University of the Witwatersrand, Johannesburg (South Africa)).
8. Flores, C. G., Schneider, H., Dornelles, J. S., Gomes, L. B., Marcilio, N. R., & Melo, P. J. (2021). Synthesis of potassium zeolite from rice husk ash as a silicon source. *Cleaner Engineering and*

Technology, *4*, 100201. https://doi.org/10.1016/j.clet.2021.100201.

9. Gargiulo, N., Shibata, K., Peluso, A., Aprea, P., Valente, T., Pezzotti, G., & Caputo, D. (2018). Reinventing rice husk ash: Derived NaX zeolite as a high-performing CO_2 adsorbent. *International Journal of Environmental Science and Technology*, *15*, 1543-1550. https://doi.org/10.1007/s13762-017-1534-5.
10. Hassan, A. and Jaaron, A., (2021). Total quality management for enhancing organizational performance: The mediating role of green manufacturing practices. Journal of Cleaner Production, 308, pp.127366. 25 July 2021. https://doi.org/10.1016/j.jclepro.2021.127366.
11. Kordala, N., & Wyszkowski, M. (2024). Zeolite properties, methods of synthesis, and selected applications. *Molecules*, *29*(5), 1069. https://doi.org/10.3390/molecules29051069.
12. Kungu, R. E. (2022). *Synthesis and characterization of novel green chemicals from rice husks and their technological applications in environmental pollution control in Kenya* (Doctoral dissertation, JKUAT-IEET).
13. Lee, J. H., Kwon, J. H., Lee, J. W., Lee, H. S., Chang, J. H., & Sang, B. I. (2017). Preparation of high purity silica originated from rice husks by chemically removing metallic impurities. *Journal of Industrial and Engineering Chemistry*, *50*, 79-85. https://doi.org/10.1016/j.jiec.2017.01.033.
14. Liu, X., Li, Z., Chen, H., Yang, L., Tian, Y., & Wang, Z. (2016). Rice husk ash as a renewable source for synthesis of sodium metasilicate crystal and its characterization. *Research on Chemical Intermediates*, *42*, 3887-3903. https://doi.org/10.1007/s11164-015-2251-7.
15. Ma, Y., Yan, C., Alshameri, A., Qiu, X., & Zhou, C. (2014). Synthesis and characterization of 13X zeolite from low-grade natural kaolin. *Advanced Powder Technology*, *25*(2), 495-499. https://doi.org/10.1016/j.apt.2013.08.002.
16. Murge, P., Dinda, S., & Roy, S. (2019). Zeolite-based sorbent for CO2 capture: preparation and performance evaluation. *Langmuir*, *35*(46), 14751-14760. https://doi.org/10.1021/acs.langmuir.9b02259.
17. Nazir, L. S. M., Yeong, Y. F., & Sabdin, S. (2018, December). Formation of pure NaX zeolite: Effect of ageing and hydrothermal synthesis parameters. In *IOP Conference Series: Materials Science and Engineering* (Vol. 458, No. 1, p. 012002). IOP Publishing. DOI 10.1088/1757-899X/458/1/012002.
18. Pandiangan, K. D., Arief, S., Jamarun, N., & Simanjuntak, W. (2017). Synthesis of zeolite-X from rice husk silica and aluminum metal as a catalyst for transesterification of palm oil. *Journal of Materials and Environmental Science*, *8*(5), 1797-1802. DOI 10.1088/1742-6596/1338/1/012015.
19. Purnomo, C. W., Salim, C., & Hinode, H. (2012). Synthesis of pure Na–X and Na–A zeolite from bagasse fly ash. *Microporous and Mesoporous Materials*, *162*, 6-13.

https://doi.org/10.1016/j.micromeso.2012.06.007.

20. Rahman, M. M., Hasnida, N., & Nik, W. W. (2009). Preparation of zeolite Y using local raw material rice husk as a silica source. *Journal of Scientific Research*, *1*(2), 285-291. https://doi.org/10.1016/j.micromeso.2012.06.007.

21. Riaz, R., Bashir, M., Imtiaz, K., Rahdar, A., Nazar, M. F., Sumrra, S. H., ... & Zafar, M. N. (2024). Silicones and their applications. In *Advances in Minerals Research* (pp. 131-156). Cham: Springer Nature Switzerland. https://doi.org/10.1007/978-3-031-49175-7_5.

22. Saceda, J. J. F., Leon, R. L. D., Rintramee, K., Prayoonpokarach, S., & Wittayakun, J. (2011). Properties of silica from rice husk and rice husk ash and their utilization for zeolite Y synthesis. *Quimica Nova*, *34*, 1394-1397. https://doi.org/10.1590/S0100-40422011000800018 .

23. Saleh, N. J., Al-Zaidi, B. Y. S., & Sabbar, Z. M. (2018). A comparative study of Y zeolite catalysts derived from natural and commercial silica: Synthesis, characterization, and catalytic performance. *Arabian Journal for Science and Engineering*, *43*, 5819-5836. https://doi.org/10.1007/s13369-017-3014-0.

24. Santasnachok, C., Kurniawan, W., Salim, C., & Hinode, H. (2014). The utility of rice husk ash from biomass power plant: synthesis of Na-A and Na-X zeolites using the two step method hydrothermal. *Journal of Advanced Agricultural Technologies Vol*, *1*(2). DOI:10.12720/joaat.1.2.75-81.

25. Saravanan, M., Sudalai, S., Dharaneesh, A. B., Prahaaladhan, V., Srinivasan, G., & Arumugam, A. (2023). An extensive review on mesoporous silica from inexpensive resources: Properties, synthesis, and application toward modern technologies. *Journal of Sol-Gel Science and Technology*, *105*(1), 1-29. https://doi.org/10.1007/s10971-022-05983-x.

26. Seghir, B. B., Hemmami, H., Hocine, B. M. E., Soumeia, Z., Sharifi-Rad, M., Awuchi, C. G., & Messaoudi, M. (2023). Methods for the preparation of silica and its nanoparticles from different natural sources. *Biological Trace Element Research*, *201*(12), 5871-5883. https://doi.org/10.1007/s12011-023-03628-w.

27. Setthaya, N., Pindi, C., Chindaprasirt, P., & Pimraksa, K. (2013). Synthesis of faujasite and analcime using of rice husk ash and metakaolin. *Advanced Materials Research*, *770*, 209-212. https://doi.org/10.4028/www.scientific.net/AMR.770.209.

28. Srisainath, R., Senthilkumar, R., & Sunder Selwyn, T. (2023). Performance and emission analysis on gasoline engine fuelled with pyrolysis oil produced from waste plastic using rice husk ash as catalyst. *International Journal of Ambient Energy*, *44*(1), 88-95. https://doi.org/10.1080/01430750.2022.2111347.

29. Wang, Y., Jia, H., Chen, P., Fang, X., & Du, T. (2020). Synthesis of La and Ce modified X zeolite

from rice husk ash for carbon dioxide capture. *Journal of Materials Research and Technology*, *9*(3), 4368-4378. https://doi.org/10.1016/j.jmrt.2020.02.061.

30. Wittayakun, J., Khemthong, P., & Prayoonpokarach, S. (2008). Synthesis and characterization of zeolite NaY from rice husk silica. *Korean Journal of Chemical Engineering*, *25*, 861-864. https://doi.org/10.1007/s11814-008-0142-y.
31. Yuvakkumar, R., Elango, V., Rajendran, V., & Kannan, N. (2014). High-purity nano silica powder from rice husk using a simple chemical method. *Journal of experimental nanoscience*, *9*(3), 272-281. https://doi.org/10.1080/17458080.2012.656709.
32. Zhang, X., Tang, D., Zhang, M., & Yang, R. (2013). Synthesis of NaX zeolite: Influence of crystallization time, temperature and batch molar ratio SiO2/Al2O3 on the particulate properties of zeolite crystals. *Powder Technology*, *235*, 322-328. https://doi.org/10.1016/j.powtec.2012.10.046.
33. Zou, Y., & Yang, T. (2019). Rice husk, rice husk ash and their applications. In *Rice bran and rice bran oil* (pp. 207-246). https://doi.org/10.1016/B978-0-12-812828-2.00009-3.